FULL PAPER

Magnetic Resonance in Medicine 00:000–000 (2015)

Ultrahigh Field Single-Refocused Diffusion Weighted Imaging Using a Matched-Phase Adiabatic Spin Echo (MASE)

Hadrien Dyvorne, Rafael O'Halloran, and Priti Balchandani

Purpose: To improve ultrahigh field diffusion-weighted imaging (DWI) in the presence of inhomogeneous transmit B_1 field by designing a novel semi-adiabatic single-refocused DWI technique.

Methods: A 180° slice-selective, adiabatic radiofrequency (RF) pulse of 4 ms duration was designed using the adiabatic Shinnar-Le Roux algorithm. A matched-phase slice-selective 90° RF pulse of 8 ms duration was designed to compensate the nonlinear phase of the adiabatic 180° RF pulse. The resulting RF pulse combination, matched-phase adiabatic spin echo (MASE), was integrated into a single-shot echo planar DWI sequence. The performance of this sequence was compared with single-refocused Stejskal-Tanner (ST), twice-refocused spin echo (TRSE) and twice-refocused adiabatic spin echo (TRASE) in simulations, phantoms, and healthy volunteers at 7 Tesla (T).

Results: In regions with inhomogeneous B_1, MASE resulted in increased signal intensity compared with ST (up to 64%). Moderate increase in specific absorption rate (35–39%) was observed for adiabatic RF pulses. MASE resulted in higher signal homogeneity at 7T, leading to improved visualization of measures derived from diffusion-weighted images such as white matter tractography and track density images.

Conclusion: Efficient adiabatic SLR pulses can be adapted to single-refocused DWI, leading to substantially improved signal uniformity when compared with conventional acquisitions. **Magn Reson Med 000:000–000, 2015. © 2015 Wiley Periodicals, Inc.**

Key words: diffusion; DWI; DTI; brain; tractography; radiofrequency; adiabatic; RF pulse; matched phase; B1; ultrahigh field; 7T diffusion

INTRODUCTION

The 7 Tesla (T) MRI scanners have the potential to improve techniques such as diffusion-weighted imaging (DWI) by providing increased signal-to-noise ratio (SNR) when compared with 3T scanners. However, several physical effects, including severe inhomogeneity of the static field (B_0) and transmit radiofrequency (RF) field (B_1) and decreased tissue T_2 values, stand in the way of performing robust DWI acquisitions at 7T. B_1 variations across the imaging volume lead to signal intensity artifacts that become more severe when using RF pulses with large flip angles, such as the 180° RF pulse used to generate a single (1) or twice refocused (2) spin echo in DWI sequences. Shorter T_2 values for brain tissue at 7T (45–50 ms as compared to 56–69 ms at 3T (3)) further affect the achievable SNR gain. Parallel transmit (PTx) systems, which exploit the added degree of freedom afforded by multiple transmit coils, may be used to achieve uniform transmit B1 profiles (4–6). However, safety limits currently restrict PTx to the use small flip angles in vivo because the heterogeneous SAR profiles resulting from parallel transmission are difficult to model. Given the high flip angles required for refocusing, PTx is not readily translatable to diffusion MRI. Additionally, such an approach requires additional specialized hardware. Dielectric pads are valuable to improve B_1 homogeneity and alter the transmit profile in a given region of the brain, but optimum placement around the subject's head is difficult to predict. The effects of B_1 inhomogeneity can also be alleviated by using adiabatic RF pulses, which operate over a wider range of B_1 values. In previous preclinical and human studies a pair of adiabatic refocusing pulses in a twice-refocused adiabatic spin-echo (TRASE) DWI acquisition achieved more uniform signal intensity in the presence of B_1 variation at high magnetic fields when compared with a conventional twice-refocused spin-echo (TRSE) approach (7,8). However, the relatively long echo time (TE) of the TRSE and TRASE DWI sequences limit the SNR gain that may be achieved at 7T. In addition, using two refocusing pulses substantially increases RF power deposition as measured by the specific absorption rate (SAR), which reduces volume coverage or results in a longer acquisition time at 7T. Given these limitations, our goal is to use a single-refocused DWI preparation (1) that offers reduced TE and SAR, combined with an adiabatic 180° RF pulse to reduce the effect of inhomogeneous B_1.

Although adiabatic refocusing pulses are typically used in a paired configuration to refocus the nonlinear phase deposited across the slice, investigators have also developed single-refocused adiabatic spin-echo sequences, using "matched-phase" 90° RF pulses that are designed to compensate the nonlinear phase induced by a single adiabatic refocusing pulse (9,10). Such methods allow the implementation of a matched-phase adiabatic spin echo (MASE) sequence, which can then be used to perform single-refocused DWI with adiabatic refocusing pulses. The purpose of this study is to develop a single-

Translational and Molecular Imaging Institute, Icahn School of Medicine at Mount Sinai, New York, New York, USA.

Grant sponsor: NIH-NINDS; Grant number: R00 NS070821; Grant sponsor: Icahn School of Medicine Capital Campaign, Translational and Molecular Imaging Institute and Department of Radiology, Icahn School of Medicine at Mount Sinai, Siemens Healthcare.

*Correspondence to: Hadrien Dyvorne, Ph.D., Translational and Molecular Imaging Institute, Icahn School of Medicine at Mount Sinai, New York NY 10029.
E-mail: hadrien.dyvorne@mountsinai.org

Received 30 January 2015; revised 27 April 2015; accepted 30 April 2015
DOI 10.1002/mrm.25790
Published online 00 Month 2015 in Wiley Online Library (wileyonlinelibrary.com).

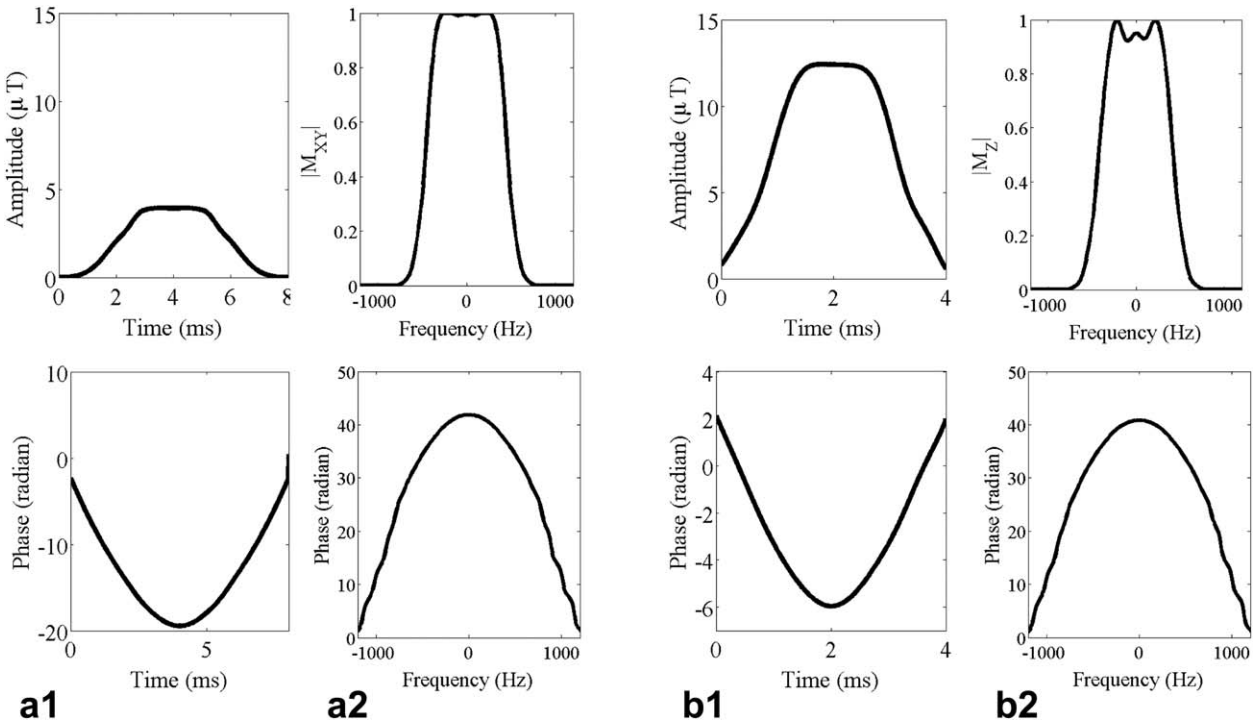

FIG. 1. RF pulse waveforms (A1,B1) and spectral profiles (A2,B2). Top: magnitude, bottom: phase. **A1,A2:** Matched-phase excitation pulse. **B1,B2:** Semi-adiabatic SLR refocusing pulse.

refocused MASE DWI sequence using an optimized slice-selective semi-adiabatic refocusing pulse coupled with a matched-phase excitation pulse, and to compare its performance with conventional DWI using linear-phase RF pulses and with the twice-refocused techniques TRSE and TRASE at 7T.

METHODS

RF Pulse Design

Semi-adiabatic pulses, which are a class of quadratic phase pulses allowing to trade-off adiabaticity, pulse length and deposited power, were designed using the adiabatic Shinnar-Le Roux (SLR) algorithm that has been previously described in detail (11). Here we briefly give the design steps leading to the refocusing pulses used in this work. First, a filter was generated using the firls function in Matlab (R2014a, The Mathworks, Natick, MA), with inputs as follows:

$$F = \text{firls}(N, F, A, W)$$

with N = 355 samples, F = [0, 0.007, 0.017, 1], and A = [1, 1, 0, 0], which represent the relative low-pass filter frequency band edges and amplitude values; and W= [0.1/8, sqrt(0.01/2)], which contains the relative ripple amplitudes in the pass-band and stop-band, respectively. Before SLR inversion, quadratic phase was applied using k=3000 cycles to induce adiabatic behavior and distribute RF energy more uniformly, reducing peak B_1 amplitude. After SLR inversion, the pulse was truncated, resulting in a 4 ms duration, 1.32 kHz bandwidth, and 12.4 μT peak amplitude at adiabatic threshold putting the peak amplitude well below the 24 μT maximum amplitude allowed on our head transmit coil at 7T.

Matched-phase excitation pulse: In a second step, a 90° excitation RF pulse was created to compensate the phase of the 180° adiabatic refocusing pulse. To achieve this, the beta polynomial of the 90° pulse was derived from that of the 180° pulse, such that:

$$\beta_{90} = (\beta_{180})^2 / \sqrt{2}$$

The corresponding minimum-phase alpha polynomial α_{90} was then generated, and the pulse envelope was derived using the inverse SLR transform. The resulting 90° pulse had an 8 ms duration, 1.43 kHz bandwidth, and 3.9 μT peak amplitude. RF pulse waveforms are shown in Figure 1.

Implementation in a DWI sequence: The complete pulse sequence diagram, showing the matched-phase spin echo inserted into a diffusion-weighted echo planar imaging (EPI) sequence, is provided in Figure 2. To correct for Nyquist ghosting occurring in EPI readouts, phase correction needs to be performed using additional calibration scans (12). In our implementation, three calibration lines are acquired in the fast readout direction at the center of k-space. In conventional diffusion-weighted EPI these lines are typically placed after the initial 90° pulse. For a matched-phase spin echo, doing so would result in nonlinear phase present in the calibration lines, which would affect ghosting reduction techniques. To address this issue, the calibration lines were acquired outside the DWI acquisition by playing a low flip angle (5°) linear-phase RF pulse before the 90° pulse. This allows the acquisition of high fidelity calibration data

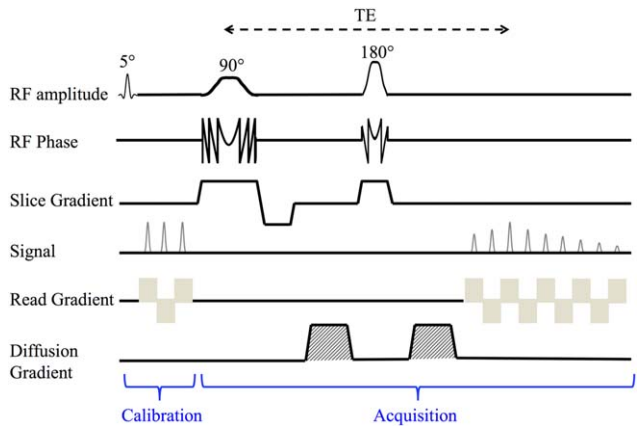

FIG. 2. Sequence diagram showing RF amplitude, RF phase and gradient waveforms for MASE diffusion sequence.

while negligibly affecting the signal available for DWI acquisition.

Simulations

The magnetization response to different RF pulses was modeled using the Cayley-Klein polynomials α and β of the respective pulses (13), neglecting the effect of transverse and longitudinal relaxation. With this formalism, an inversion or refocusing pulse transforms the magnetization as follows:

$$M(+) = \beta_{180}{}^2 M(-)$$

where M(−) and M(+) represent the magnetization before and after the pulse respectively, and (*) stands for the complex conjugate. Given an initial magnetization M_0, the transverse magnetization after the 90° excitation pulse is

$$M_{xy} = 2\,\alpha_{90}{}^*\beta_{90} M_0$$

Finally, the magnetization at the echo time for a single spin echo sequence is:

$$M_{SE} = (2\,\alpha_{90}{}^*\beta_{90})^*\beta_{180}{}^2 M_0$$

For each pulse, the frequency-dependent parameters α and β were computed as a function of the applied B_1 field, ranging from 0.5 to 2.5 times the optimal B_1 value (defined as the B_1 necessary to achieve a given rotation for linear pulses, or B_1 at adiabatic threshold for adiabatic pulses). The resulting frequency (or slice) profiles were then integrated to yield the total spin echo signal as a function of B_1.

MR Imaging

The 7T imaging was performed on an actively shielded, whole-body Siemens Magnetom 7T scanner (Siemens Healthcare, Erlangen, Germany) equipped with a 32-channel receive / 1 channel transmit head coil (Nova Medical, Wilmington, MA) and 70 mT/m maximum gradient (200 mT/m/ms slew rate). B_0-shimming was performed to the 2nd order on a manually adjusted volume. Transmitter voltage was adjusted as follows: average flip angle was measured using the Bloch-Siegert shift technique (11) over a 5 cm × 5cm region located in a central part of the brain. The voltage was then adjusted to calibrate the average flip angle value in this region, resulting in transmitter voltages of order 200 V. Figure 4A shows a Bloch-Siegert acquisition in a volunteer. Calibration of the adiabatic pulses was experimentally performed on a spherical phantom containing a 0.011 g/L solution of MACROLEX Blue (Fig. 4B). First the refocusing pulse was calibrated using the TRASE sequence by increasing the amplitude of the adiabatic pulses (keeping the excitation pulse amplitude constant) until a plateau was reached for signal intensity. The matched-phase excitation pulse of MASE was then adjusted to match the previously calibrated adiabatic refocusing pulse. The excitation pulse amplitude was varied until a maximum in signal intensity was reached (Fig. 4B). Anatomical T_1-weighted images were acquired in a sagittal orientation using a three-dimensional (3D) MP-RAGE sequence (14,15). The following diffusion acquisitions were performed in this order: ST, MASE, TRSE, and TRASE. Thirty slices were sampled in axial direction with anterior–posterior phase encoding and a partial Fourier ratio of 6/8. Parallel imaging was applied using GRAPPA (16) with acceleration factor R=3. Each sequence was run at the maximum SAR, within limits set by the Food and Drug Administration regulations (12 W/kg average SAR for local head exposure). Increased RF power that resulted when using adiabatic pulses or twice-refocused acquisitions was balanced with an increase in TR to maintain similar average SAR. TE/TR were 51/9700 ms for ST, 53/13500 ms for MASE, 65/15200 ms for TRSE, and 65/20500 ms for TRASE.

Phantom Acquisitions

Phantom experiments were performed on a 170 mm-diameter sphere containing saline solution (with concentrations [NaOH] = 56 mM, [KH_2PO_4] = 50 mM) and used as a model for the human head.

In Vivo Acquisitions

In vivo experiments were performed on healthy volunteers. In one experiment, all four DWI acquisitions (ST, MASE, TRSE, and TRASE) were performed on the same subject using 20 diffusion directions (b = 1000 s/mm^2), with spatial resolution 1.9 × 1.9 × 3 mm^3. In a second scan, 68 diffusion directions were acquired (b = 1000 s/mm^2) with higher spatial resolution (1.4 × 1.4 × 2 mm^3). For the second in vivo acquisition, only the single-refocused DWI acquisitions (ST and MASE) were acquired to determine the benefit of MASE for tractography and track density imaging within a reasonable total exam time. Acquisition times for the 68-directions scans were 10:51 min for ST (TR 8.8 s) and 15:10 min for MASE (TR 12.3 s).

Diffusion Data Analysis

Adiabatic acquisitions were compared with conventional acquisitions in terms of signal intensity, which was measured on reconstructed diffusion trace images instead of individual diffusion directions to avoid anisotropic effects. Signal intensity could be directly compared

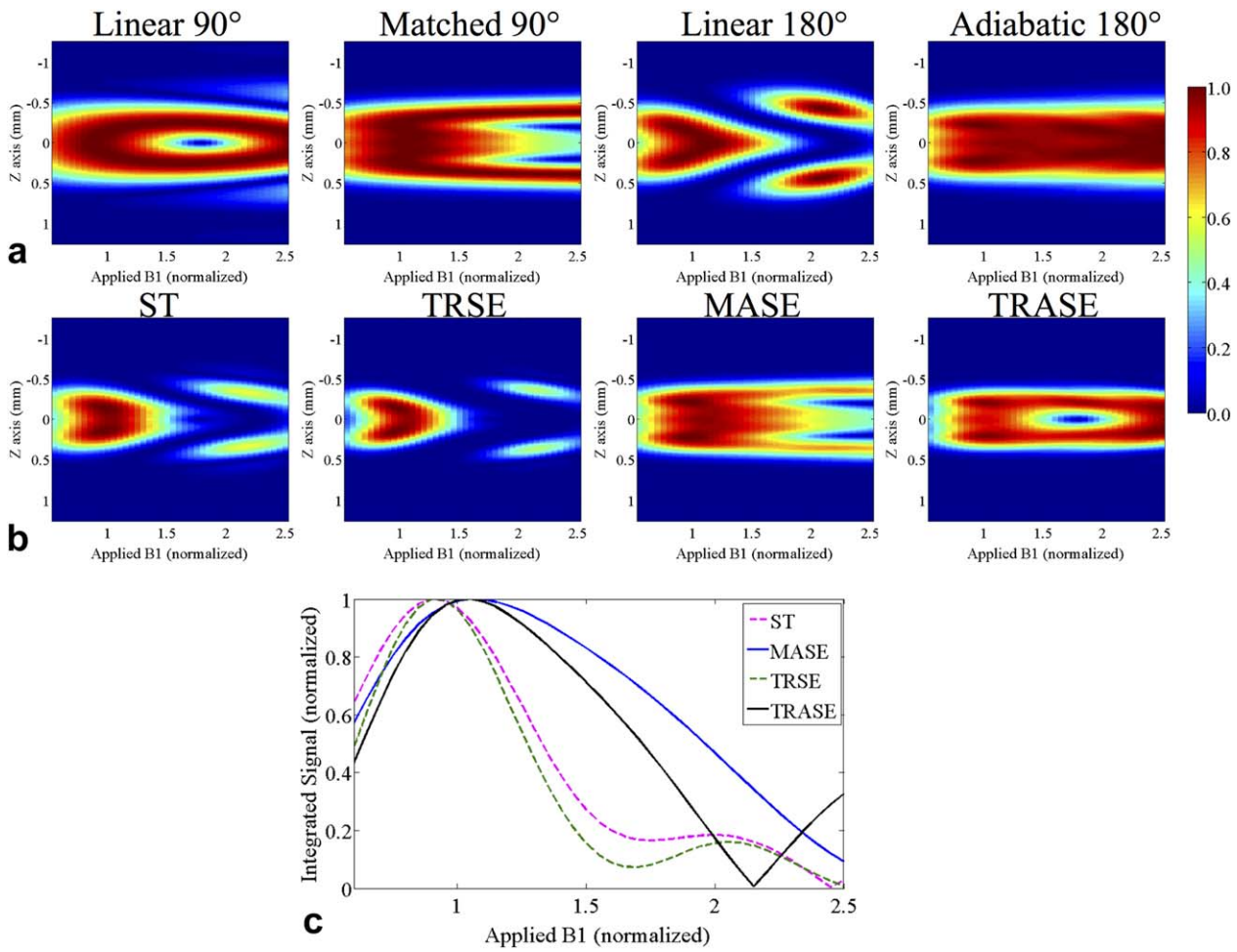

FIG. 3. Simulated behavior of different RF pulses as a function of normalized applied B_1 ($B_1 = 1$ corresponds to RF amplitude required to achieve 180° rotation for linear refocusing pulses or to reach adiabatic threshold for adiabatic pulses). **A:** Magnetization profiles for linear 90°, matched-phase 90°, linear 180°, and adiabatic 180° (from left to right). **B:** Spin echo magnetization profiles for ST, TRSE, MASE, and TRASE methods (from left to right). **C:** Spin echo signal integrated over the slice (taking into account phase-matching deterioration). Both MASE and TRASE yield improved spin echo signal for a wider range of B_1 values, when compared with ST and TRSE.

because the receive gains and subject position relative to receive coils were identical between the DWI scans. Pixel-by-pixel division was performed between adiabatic and conventional acquisitions, as well as between single and twice refocused acquisitions, to derive maps showing signal enhancement. A signal intensity profile was extracted along a horizontal line placed on signal enhancement maps, using custom-built analysis software designed with Matlab (R2014a, Mathworks, Natick, MA).

In addition to signal intensity comparison, we compared the performance of different diffusion acquisitions in terms of the derived diffusion metrics. Diffusion-weighted volumes were registered to anatomical MP-RAGE images and corrected for eddy current-induced bias using the FMRIB Software Library (FSL) (17). Further DWI processing was achieved using MRtrix (18,19). Fractional anisotropy (FA) was derived from the intensity-masked DW images for both 20 and 68-direction acquisitions. White matter tractography and track density imaging (TDI) (20) were performed on the 68-direction datasets, using the constrained spherical deconvolution method (21).

Tractography

Next, the effect of the adiabatic RF pulses on fiber tractography was evaluated on the 68-direction datasets. Tracks were generated using a hand-drawn seed region of interest (ROI), and were constrained to include hand-drawn target ROIs. For exact technique comparison, all tracking parameters and ROIs were the same for ST and MASE datasets. We evaluated tractography performance on a group of fibers that passes through the region most severely affected by B_1 inhomogeneity, running from the ventral tegmental area (VTA) to the frontal cortex by means of the anterior limb of the internal capsule (ALIC). Tracks were generated from a seed ROI placed in the midbrain-VTA region, and an include ROI in the ALIC, in both the left and right hemispheres. For the left and right side pathways probabilistic tractography was performed, generating 10,000 tracks from the seed region and accepting only tracks passing through the include region. Finally, track density imaging (TDI) was derived from whole brain fiber tracking using 10^6 tracks and an isotropic spatial resolution of 1.5 mm.

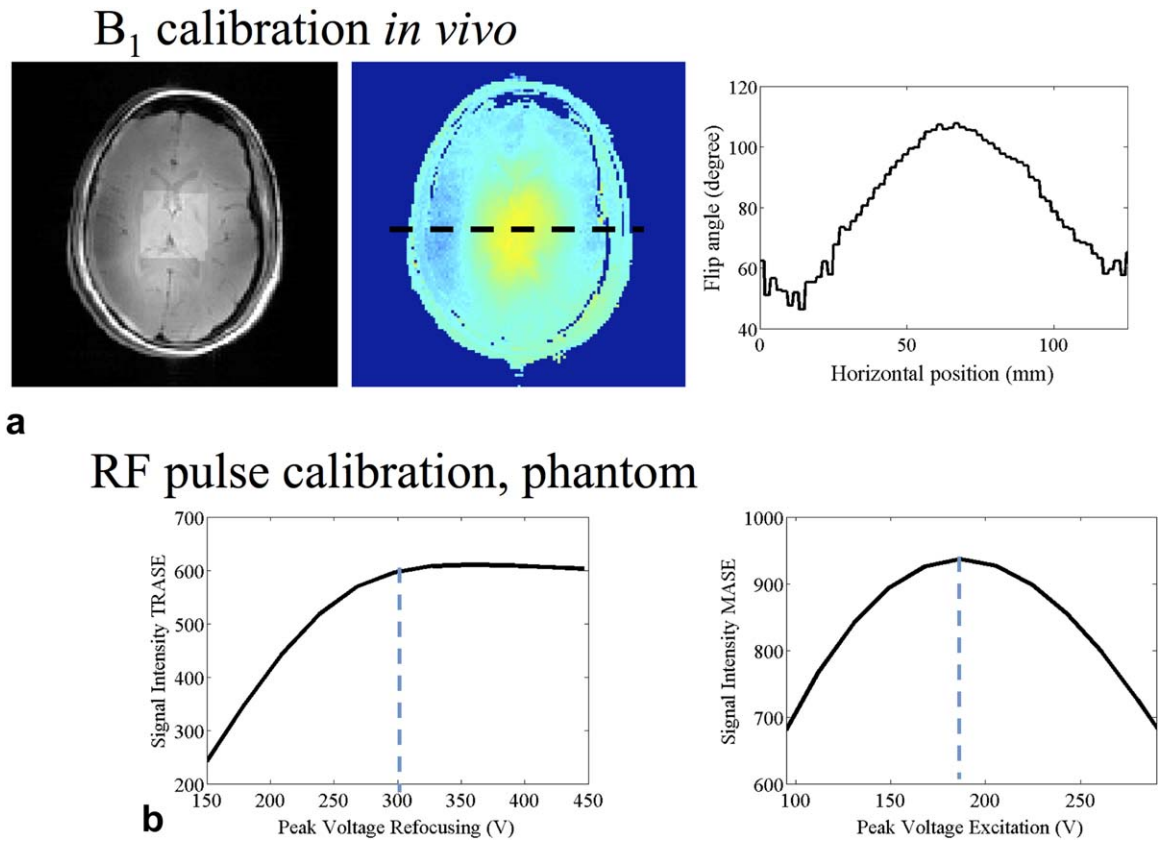

FIG. 4. Calibration routines for transmitter voltage and adiabatic pulses. **A:** In vivo Bloch-Siegert acquisition showing ROI used for flip angle calibration (left, bright box on the magnitude image), flip angle map (middle) and flip angle values along a horizontal profile in the brain of a healthy volunteer. **B:** RF pulse calibration for adiabatic DWI sequences in a MACROLEX oil phantom (dashed lines indicate operating voltages). Left: refocusing pulse calibration using TRASE, leading to an operating voltage of 300 V at the adiabatic plateau. Right: matched-phase excitation pulse calibration.

RESULTS

Simulation Results for Spin Echo Magnetization

Figure 3 shows the magnetization and signal as a function of the frequency and applied B_1, for individual pulses as well as full spin echoes. For both MASE and TRASE, the spin echo signal integrated over the slice is higher than for conventional ST and TRSE in a wide range of B_1 values. This is because, for any B_1 over the adiabatic threshold, the profile of the adiabatic refocusing pulse (Figure 3A, right panel) remains almost unchanged, while the conventional refocusing pulse profile demonstrates severe variations. The deleterious effects of the conventional refocusing pulse also result in worse behavior for TRSE when compared with ST, because TRSE uses two refocusing pulses, compounding their effects. Significant differences are also observed between conventional and matched-phase excitation pulses. Because a conventional excitation pulse suffers from severe signal loss at 1.5-2 B_1 overdrive, while a matched-phase excitation pulse offers an improved slice profile over this range, the MASE technique yields higher spin echo signal than TRASE over a large B_1 range (Figs. 3B,C).

Phantom Results

In Figure 5, central axial slices from the trace-weighted ($b = 1000$ s/mm^2) volume acquired in the water phantom using ST (Fig. 5A1), MASE (Fig. 5A2), TRSE (Fig. 5B1), and TRASE (Fig. 5B2) are compared. Both of the nonadiabatic preparations (Fig. 5A1,B1) have lower signal in the center of the image than their adiabatic counterparts (Fig. 5A2,B2), demonstrating the enhanced uniformity of the adiabatic pulses. In an image of the ratio of the image acquired with each adiabatic pulse to the image acquired with its non-adiabatic counterpart, it can been appreciated that the signal uniformity is primarily improved in the center of the image (Fig. 5C1,D1) with little change in the periphery of the image. A horizontal profile across the ratio images is plotted in Figures 5C2,D2 to show the shape and magnitude of the improvement obtained with adiabatic preparations. The signal in the center of the image up to 90% higher for MASE versus ST, up to 130% higher for TRASE versus TRSE. Finally, the image ratio between MASE and TRASE in Figures 5E1,E2 shows that adiabatic acquisitions yield similar signal in a saline phantom.

In Vivo Results

In Figure 6, signal intensities on the trace-weighted images acquired in vivo with each of the preparations are compared. The images from left to right are the trace-weighted image acquired with the nonadiabatic sequence (Figure 6, first column), the trace-weighted image acquired with the adiabatic sequence (Figure 6, second

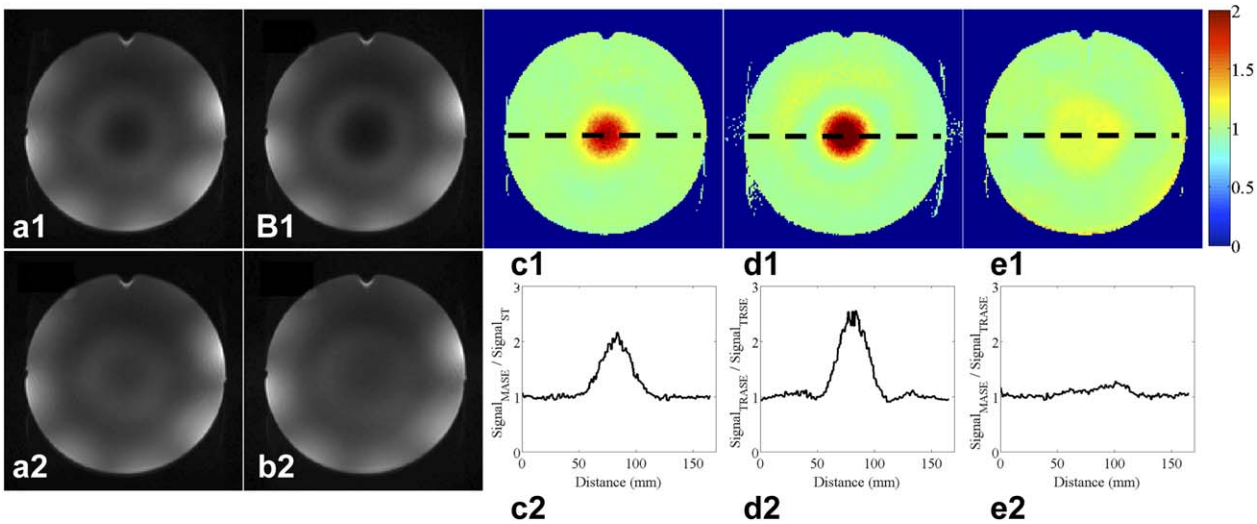

FIG. 5. Comparison between adiabatic and conventional diffusion with b value of 1000 s/mm^2 measured at 7T in a spherical head phantom. **A1:** ST acquisition. **A2:** MASE acquisition. **B1:** TRSE acquisition. **B2:** TRASE acquisition. **C1:** Ratio of MASE to ST image. **D1:** Ratio of TRASE to TRSE image. **E1:** Ratio of MASE to TRASE image. **C2,D2,E2:** Intensity profile along a horizontal diameter in C1, D1, E1.

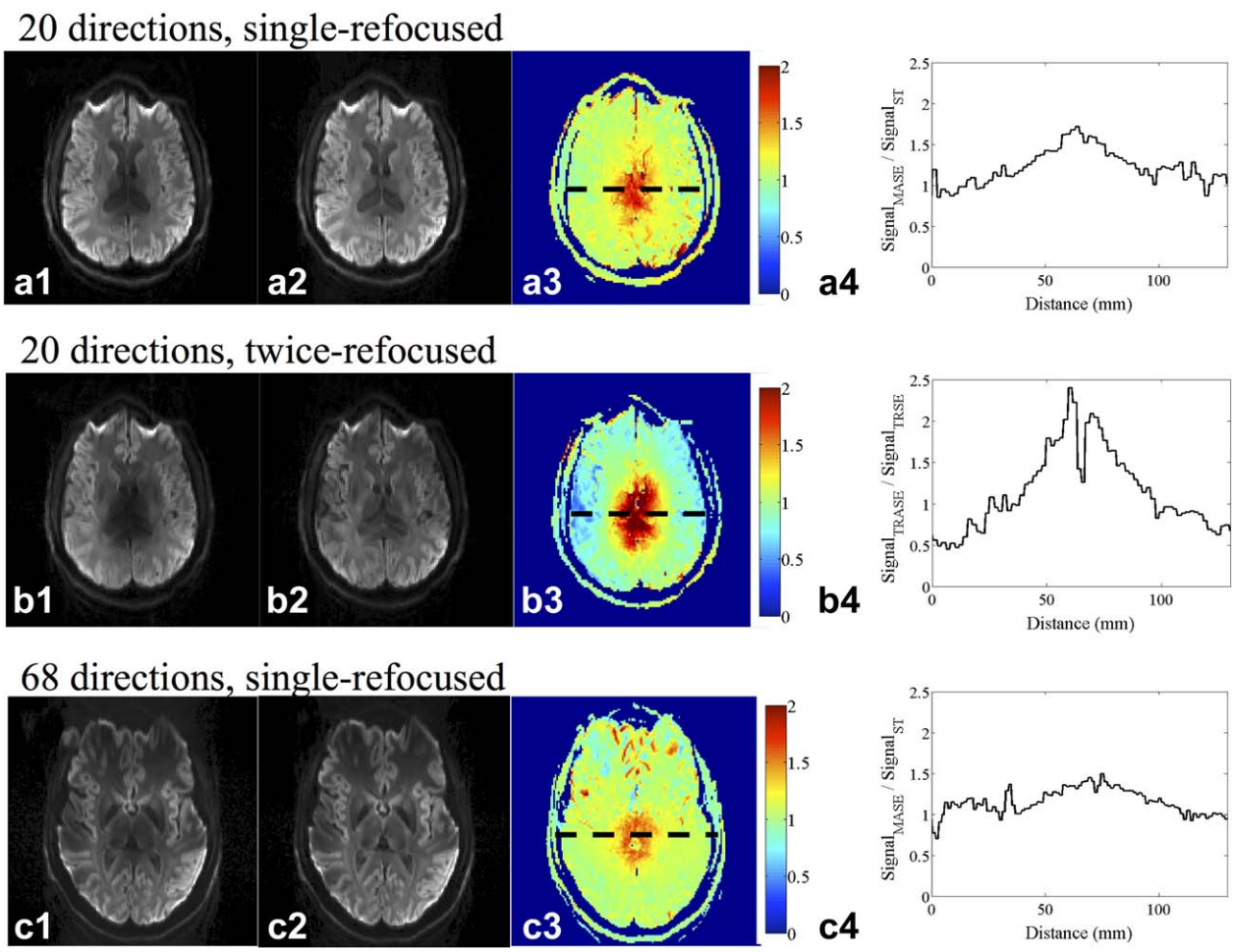

FIG. 6. Single-refocused (A) and twice refocused (B) 7T brain DWI acquired in a healthy subject, using 20 diffusion directions. C: DWI acquired in another healthy volunteer using 68 diffusion directions. **A1,A2,B1,B2:** Trace-weighted signal intensity of 20-directions ST, MASE, TRSE, and TRASE. **C1,C2:** Trace-weighted signal intensity of 68-directions ST and MASE. **A3,B3,C3:** Signal intensity ratio between adiabatic and conventional acquisitions; **A4,B4,C4:** Profiles along a horizontal line for images A3, B3 and C3 respectively. When using adiabatic refocusing pulses, the increase in signal intensity at the center of the field of view was up to 64% for MASE versus ST (20 directions), 140% for TRASE versus TRSE (20 directions) and 50% for MASE versus ST (68 directions).

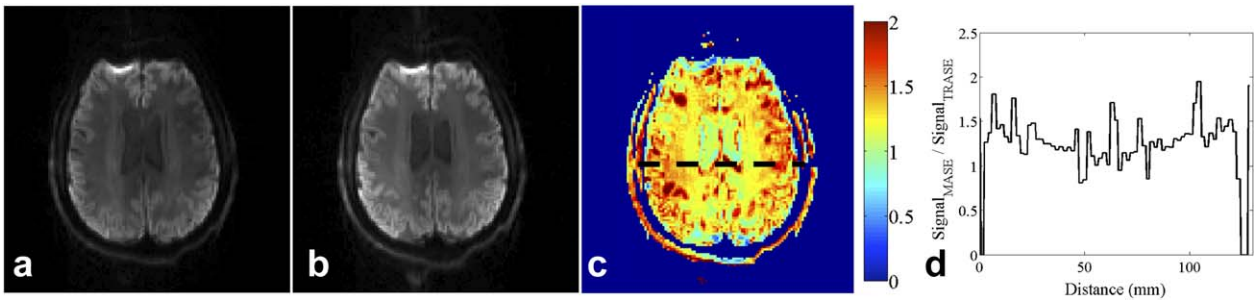

FIG. 7. Comparison of TRASE (**A**) and MASE (**B**) acquisitions: **C:** Ratio of MASE to TRASE signal intensity. **D:** profile along a horizontal line in C. In white matter regions, signal intensity is 20–40% higher for MASE compared with TRASE, as a result of the smaller echo time of single-refocused MASE acquisition.

column), the ratio of the image acquired with the adiabatic sequence to the image acquired in the nonadiabatic sequence (Figure 6, third column), and a central horizontal profile across the ratio image (Figure 6, last column).

20-Directions Brain DWI

In vivo signal intensity comparisons of all four sequences using 20-direction DWI acquisitions are shown in Figures 6A,B. Similar to the phantom experiment, higher signal intensity was observed in central regions of the brain when comparing MASE to ST or TRASE to TRSE. The gain in signal intensity was found to be higher when comparing twice-refocused acquisitions (up to 140%) than for single refocused ones (up to 64%), because using two conventional refocusing pulses led to more severe signal loss, as demonstrated in Figure 3. Finally, RF power deposition was lowest for ST, followed by MASE, TRSE, and TRASE, as reflected by their respective TRs (9.7, 13.5, 15.2, and 20.5 s) necessary to operate within SAR limits. The use of adiabatic pulses led to increased deposited power (39% for MASE versus ST and 35% for TRASE versus TRSE) as expected.

68-Directions Brain DWI

Signal intensity comparisons of the trace-weighted images acquired in MASE and ST are shown in Figure

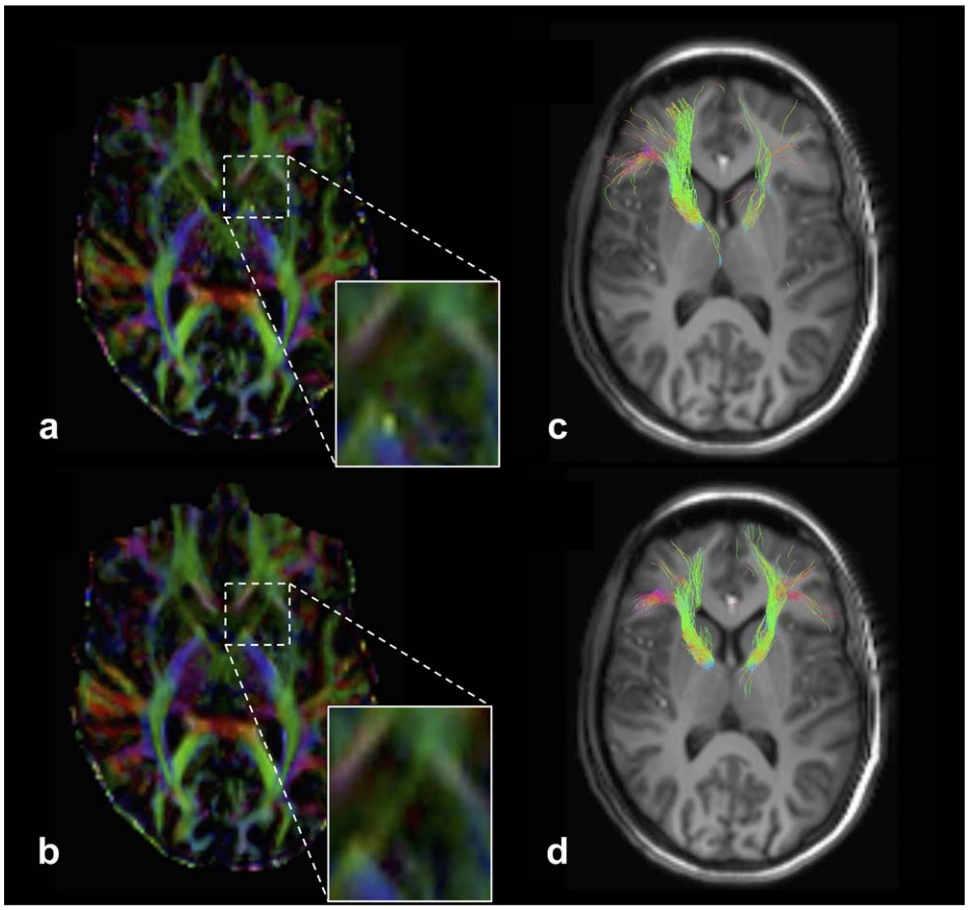

FIG. 8. Single-refocused 68-direction 7T brain DWI example. **A,B:** Fractional anisotropy (FA) for ST and MASE acquisitions. The zoomed region shows a disrupted group of fibers in the ALIC for ST acquisition, which is well represented with MASE. **C,D:** Tracks seeding from the midbrain / VTA region and including the ALIC. Poor tracking was performed with ST, as a result of signal loss in the central region. Tracks computed with MASE had a symmetric appearance (D).

6C; note that twice refocused sequences were not acquired in this subject. In this dataset, gains up to 50% signal intensity were observed in central regions, which included portions of the thalamus as well as the splenium of the corpus callosum.

In Figure 7, signal intensities between MASE and TRASE are compared for the 20-direction dataset, to evaluate the advantage of lower echo time achievable with MASE. In the signal intensity ratio image between MASE and TRASE, shown in Figure 7C, globally higher signal of MASE acquisition is observed. The line profile (Fig. 7D) shows that in white matter regions the MASE signal intensity is 20 to 40% higher than that of TRASE.

White Matter Tractography and Track Density Imaging

In Figure 8, axial slices of the principle eigenvector image weighted by FA (color FA) and fiber tractography from the data acquired using the 68-direction protocol with MASE and ST are compared. In the zoom-in of the color FA the better depiction of the ALIC on MASE compared with ST is apparent (Figures 8A,B, zoom box). This is the result of low SNR in the ST acquisition; noise propagates through the calculation of the tensor resulting in changes in the derived parametric maps such as the color FA. The effect of this reduced SNR on the fiber tractography of the group of fibers which passes through the ALIC (Figs. 8C,D) is a reduction in the number of tracks found in the ST data compared with the MASE data, especially apparent on the left side. The tracks obtained from the MASE data, by contrast, are symmetric in appearance as expected in this healthy subject.

In Figure 9, a trace-weighted central slice and coronal reformat (Figures 9A,C) of the 68-direction acquisitions and corresponding TDI (Figures 9B,D) from the ST and MASE acquisitions are compared. As noted previously, the image acquired with the ST acquisition has lower signal in the center part of the image than the image acquired with the MASE acquisition. The consequences of this reduction in signal on the tractography can be seen in the TDI (Figs. 9B,D). The most obvious differences are in the regions affected by the signal loss, with higher densities of tracks in the central region of the brain and the ALIC (Figure 9, arrows) in the TDI generated from the MASE data compared with the TDI generated from the ST data. However, because tractography uses data from multiple regions to generate tracks, differences are also visible in regions not directly affected by the signal intensity loss such as the right frontal region indicated in Figure 9D in the upper left corner.

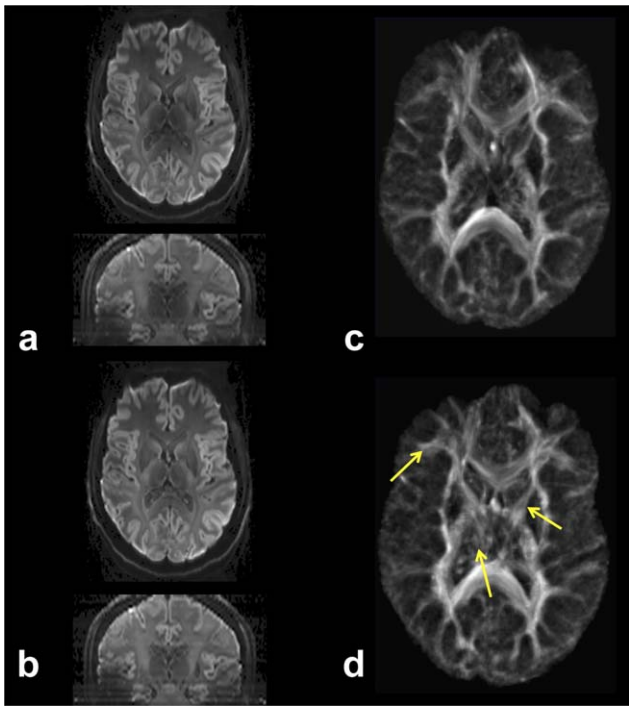

FIG. 9. **A,B:** Trace-weighted images for the 68-direction DWI datasets acquired with conventional ST and MASE respectively, showing reduced signal intensity for ST in regions near the thalamus (coronal reformatted images are also shown). **C,D:** Track density imaging derived from whole-brain tractography performed using 10^6 tracks and a resolution of 1.5 mm^3. Arrows point to increased fiber density for MASE, observed in central and frontal regions, as well as in the internal capsule.

DISCUSSION

In this study, we have developed a new single-refocused DWI acquisition which uses a MASE to achieve reduced sensitivity to B_1 variations at ultrahigh field. By comparing adiabatic and conventional single- and twice-refocused DWI acquisitions, we found that adiabatic sequences (MASE and TRASE) led to increased signal in a large range of B_1 when compared with conventional ones (ST and TRSE), as shown by simulations as well as in vivo experiments. This resulted in recovered signal in important areas of the brain and improved calculation of diffusion metrics. Furthermore, white matter tractography performed with a MASE acquisition showed improved, more symmetric track visualization compared with conventional single-refocused ST. Due to a lack of a "gold standard," typical of tractography experiments in vivo, the improvement in tractography in MASE versus ST was inferred from a more symmetric visualization of tracks in a healthy subject.

MASE yielded higher signal than twice-refocused TRASE because of shorter achievable minimum echo time. In addition, simulations showed that the matched-phase excitation pulse of MASE has a different slice profile than a conventional excitation pulse, decreasing slowly in efficiency when B_1 increases. This results in slightly improved immunity to B_1 compared with TRASE, up to approximately 2.3 overdrive factor. Finally, using MASE results in significant SAR reduction compared with TRASE. For these reasons, we believe that MASE is a better option than TRASE to reduce the effect of B_1 inhomogeneity at ultrahigh field, allowing for higher signal and reduced RF power deposition.

To assert the efficiency of the MASE approach against conventional DWI, the increase in scan time imposed by larger SAR deposition needs to be balanced against the gains in signal. With MASE, we observed signal intensity gains ranging from 50–63% in the center of the brain, where B_1 values are the highest. A comparable gain could be achieved with signal averaging, requiring in the

best case two to three averages. Thus signal averaging would lead to longer scan time when compared with the 40% increase in scan time imposed by SAR limitations. Furthermore, increased signal homogeneity may improve the diagnostic performance of DWI at high b value.

Tractography based on images acquired with MASE resulted in more fibers compared with ST for a group of fibers passing through the ALIC, as well as a more symmetric left–right representation of the tracks. Furthermore, the TDI results show that this trend holds in other regions, especially in the central region encompassing the thalamus. This has implications for structural connectivity analyses such as those proposed in human connectome projects (22). Because connectivity is based on the tractography, differences in tracking can have profound effects on the derived connectivity matrices, especially in massively connected "hub" regions like the thalamus (23–25). The tractography results shown here indicate that more uniform B_1 provided by MASE may be important in obtaining accurate connectivity measures in areas most affected by B_1 inhomogeneity such as the thalamus and the internal capsule.

The pulse pair used in MASE is very amenable to conversion into a simultaneous multislice (SMS) pulse pair. Feldman et al. have already published a SEAMS pulse pair (26) that achieves this exact purpose. Future work includes evaluating MASE in a larger cohort of subjects undergoing diffusion-weighted tractography, developing a SMS version of MASE by using a SEAMS pulse pair in a single refocused diffusion sequence, as well as combining improved readout options, such as segmented EPI (27), with adiabatic RF pulses to provide a diffusion sequence robust to both B_0 and B_1 inhomogeneity.

REFERENCES

1. Stejskal EO, Tanner JE. Spin diffusion measurements: spin echoes in the presence of a time-dependent field gradient. J Chem Phys 1965; 42:288.
2. Reese TG, Heid O, Weisskoff RM, Wedeen VJ. Reduction of eddy-current-induced distortion in diffusion MRI using a twice-refocused spin echo. Magn Reson Med 2003;49:177–182.
3. Stanisz GJ, Odrobina EE, Pun J, Escaravage M, Graham SJ, Bronskill MJ, Henkelman RM. T1, T2 relaxation and magnetization transfer in tissue at 3T. Magn Reson Med 2005;54:507–512.
4. Grissom W, Yip CY, Zhang Z, Stenger VA, Fessler JA, Noll DC. Spatial domain method for the design of RF pulses in multicoil parallel excitation. Magn Reson Med 2006;56:620–629.
5. Katscher U, Bornert P, Leussler C, van den Brink JS. Transmit SENSE. Magn Reson Med 2003;49:144–150.
6. Zhu Y. Parallel excitation with an array of transmit coils. Magn Reson Med 2004;51:775–784.
7. Balchandani P, Qiu D. Semi-adiabatic Shinnar-Le Roux pulses and their application to diffusion tensor imaging of humans at 7T. Magn Reson Imaging 2014;32:804–812.
8. van de Looij Y, Kunz N, Huppi P, Gruetter R, Sizonenko S. Diffusion tensor echo planar imaging using surface coil transceiver with a semiadiabatic RF pulse sequence at 14.1T. Magn Reson Med 2011;65:732–737.
9. Balchandani P, Khalighi MM, Glover G, Pauly J, Spielman D. Self-refocused adiabatic pulse for spin echo imaging at 7 T. Magn Reson Med 2012;67:1077–1085.
10. Park JY, Garwood M. Spin-echo MRI using pi/2 and pi hyperbolic secant pulses. Magn Reson Med 2009;61:175–187.
11. Balchandani P, Pauly J, Spielman D. Designing adiabatic radio frequency pulses using the Shinnar-Le Roux algorithm. Magn Reson Med 2010;64:843–851.
12. Ahn CB, Cho ZH. A new phase correction method in NMR imaging based on autocorrelation and histogram analysis. IEEE Trans Med Imaging 1987;6:32–36.
13. Pauly J, Le Roux P, Nishimura D, Macovski A. Parameter relations for the Shinnar-Le Roux selective excitation pulse design algorithm [NMR imaging]. IEEE Trans Med Imaging 1991;10:53–65.
14. Brant-Zawadzki M, Gillan GD, Nitz WR. MP RAGE: a three-dimensional, T1-weighted, gradient-echo sequence–initial experience in the brain. Radiology 1992;182:769–775.
15. Deichmann R, Good CD, Josephs O, Ashburner J, Turner R. Optimization of 3-D MP-RAGE sequences for structural brain imaging. Neuroimage 2000;12:112–127.
16. Griswold MA, Jakob PM, Heidemann RM, Nittka M, Jellus V, Wang J, Kiefer B, Haase A. Generalized autocalibrating partially parallel acquisitions (GRAPPA). Magn Reson Med 2002;47:1202–1210.
17. FSL. FMRIB Software Library v5.0, http://fsl.fmrib.ox.ac.uk/. Released September 2012, accessed October 2014.
18. Tournier JD. MRtrix, http://www.brain.org.au/software/mrtrix/index.html. Released February 2014, accessed August 2014.
19. Tournier JD, Calamante F, Connelly A. MRtrix: diffusion tractography in crossing fiber regions. Int J Imaging Syst Technol 2012;22:53–66.
20. Calamante F, Tournier JD, Jackson GD, Connelly A. Track-density imaging (TDI): super-resolution white matter imaging using whole-brain track-density mapping. Neuroimage 2010;53:1233–1243.
21. Tournier JD, Calamante F, Gadian DG, Connelly A. Direct estimation of the fiber orientation density function from diffusion-weighted MRI data using spherical deconvolution. Neuroimage 2004;23:1176–1185.
22. Van Essen DC, Smith SM, Barch DM, Behrens TE, Yacoub E, Ugurbil K, Consortium WU-MH. The WU-Minn Human Connectome Project: an overview. Neuroimage 2013;80:62–79.
23. Crossley NA, Mechelli A, Scott J, Carletti F, Fox PT, McGuire P, Bullmore ET. The hubs of the human connectome are generally implicated in the anatomy of brain disorders. Brain 2014;137(Pt 8): 2382–2395.
24. Sporns O. The human connectome: a complex network. Ann N Y Acad Sci 2011;1224:109–125.
25. van den Heuvel MP, Sporns O. Rich-club organization of the human connectome. J Neurosci 2011;31:15775–15786.
26. Feldman RE, Islam HM, Xu J, Balchandani P. A SEmi-Adiabatic matched-phase spin echo (SEAMS) PINS pulse-pair for B -insensitive simultaneous multislice imaging. Magn Reson Med 2015. doi: 10.1002/mrm.25654.
27. Heidemann RM, Porter DA, Anwander A, Feiweier T, Heberlein K, Knosche TR, Turner R. Diffusion imaging in humans at 7T using readout-segmented EPI and GRAPPA. Magn Reson Med 2010;64:9–14.